Supporting information for

Fluorinated- and non-fluorinated-diarylamine-Zn(II) and Cu(II) Phthalocyanines as Symmetrical vs Asymmetrical Hole Selective Materials

Adrián Hernández[a], *Naveen Harindu Hemasiri*[b], *Samrana Kazim*[b,c], Javier Ortiz[a], Shahzada Ahmad[b,c]* and Ángela Sastre-Santos[a]*

[a] *Área de Química Orgánica, Instituto de Bioingeniería, Universidad Miguel Hernández, Avda. Universidad S/N, 03202, Elche, Spain.*

[b] *BCMaterials, Basque Center for Materials, Applications, and Nanostructures, UPV/EHU Science Park, 48940, Leioa, Spain. Email: shahzada.ahmad@bcmaterials.net*

[c] *IKERBASQUE, Basque Foundation for Science, Bilbao, 48009, Spain*

Characterization of phthalonitrile 1

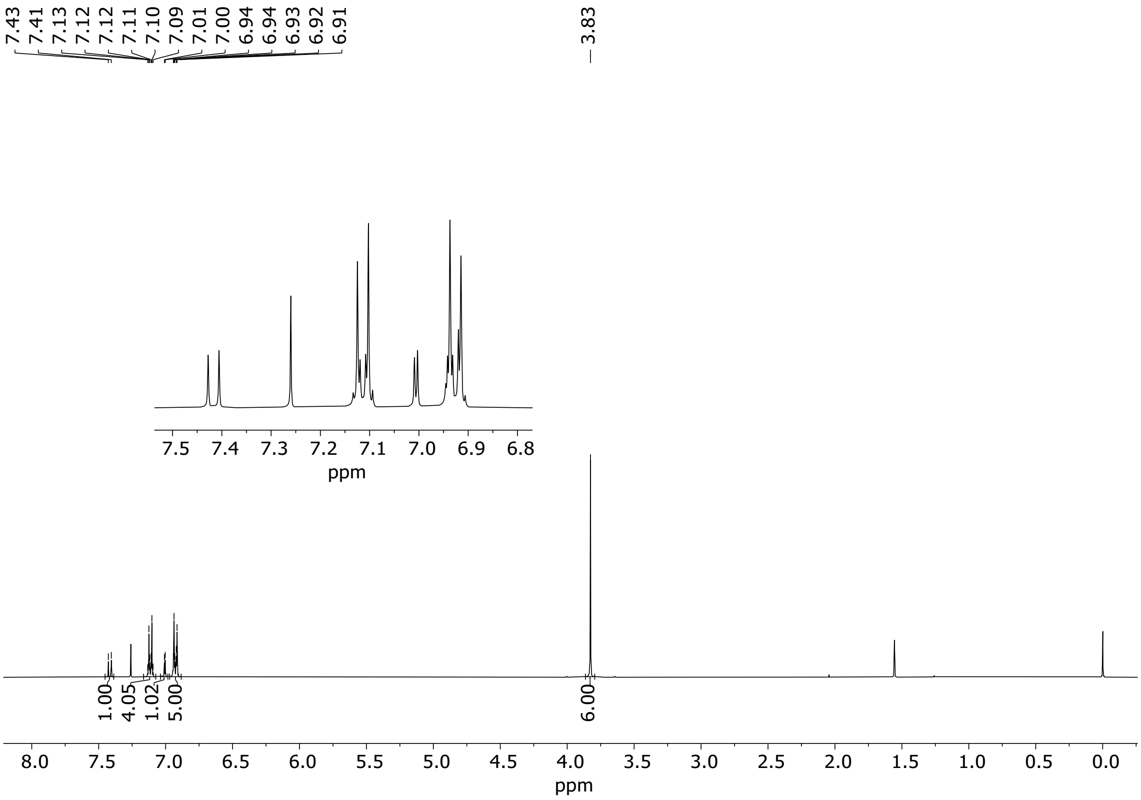

Figure S1. ^{1}H-NMR of **1** in $CDCl_3$.

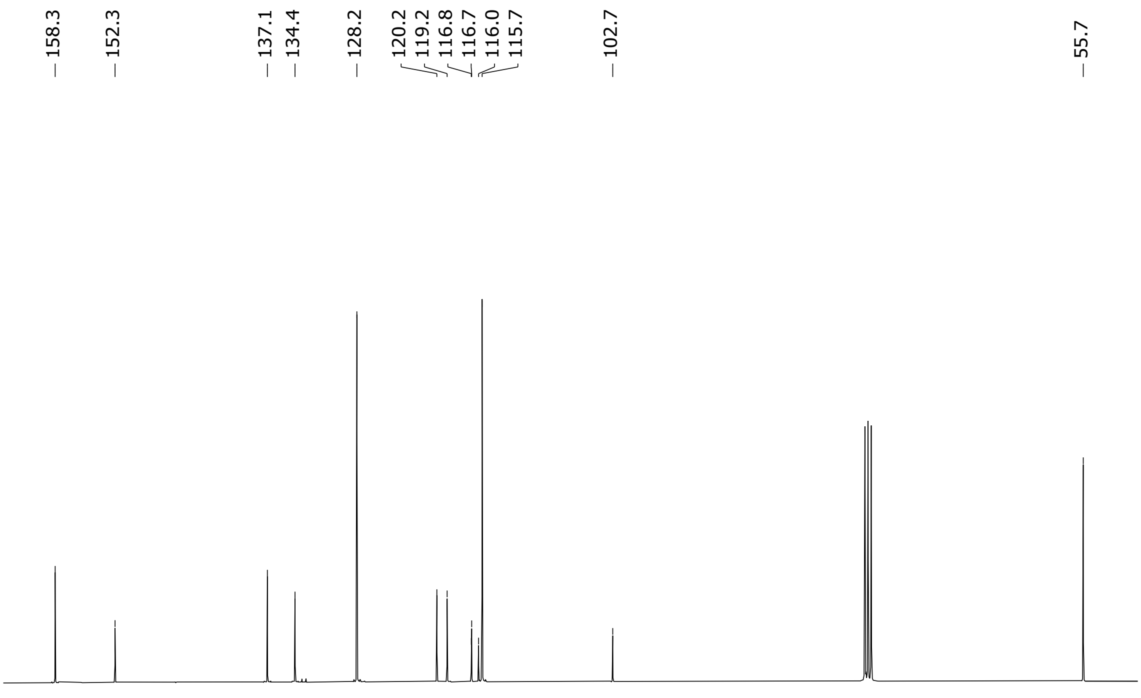

Figure S2. ^{13}C-NMR of **1** in $CDCl_3$.

Characterization of phthalonitrile 2

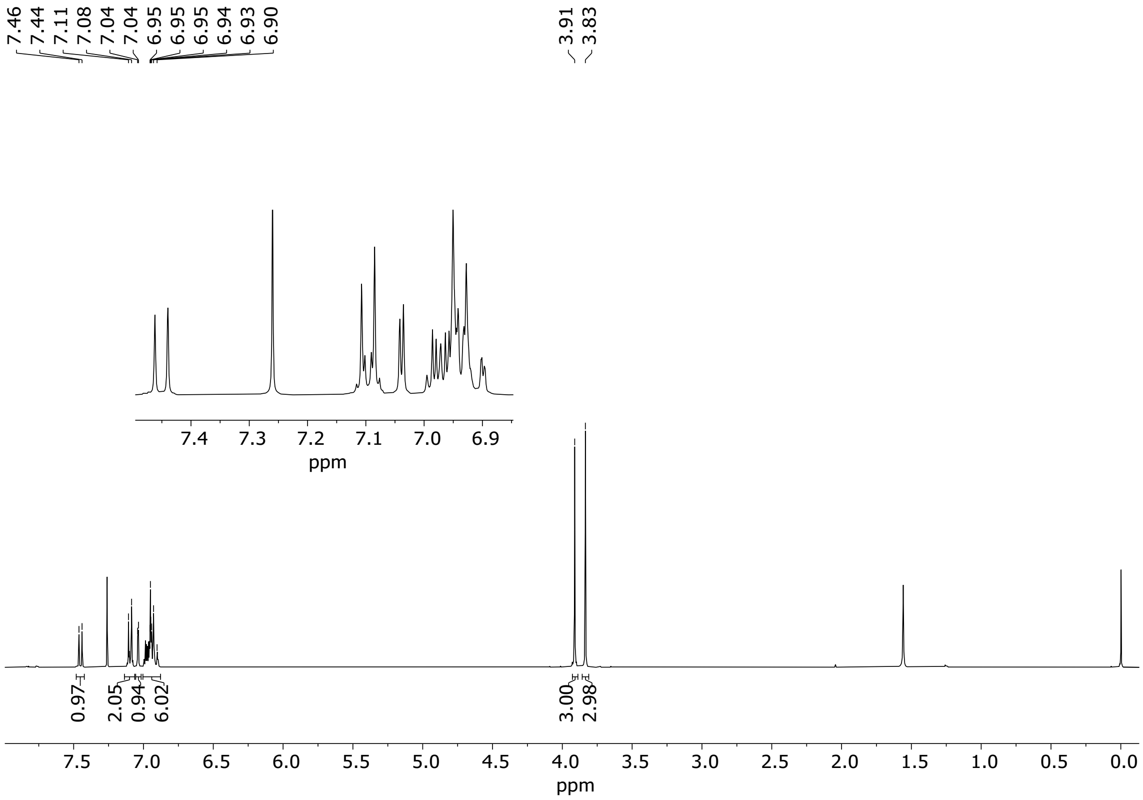

Figure S3. ^{1}H-NMR of **2** in $CDCl_3$.

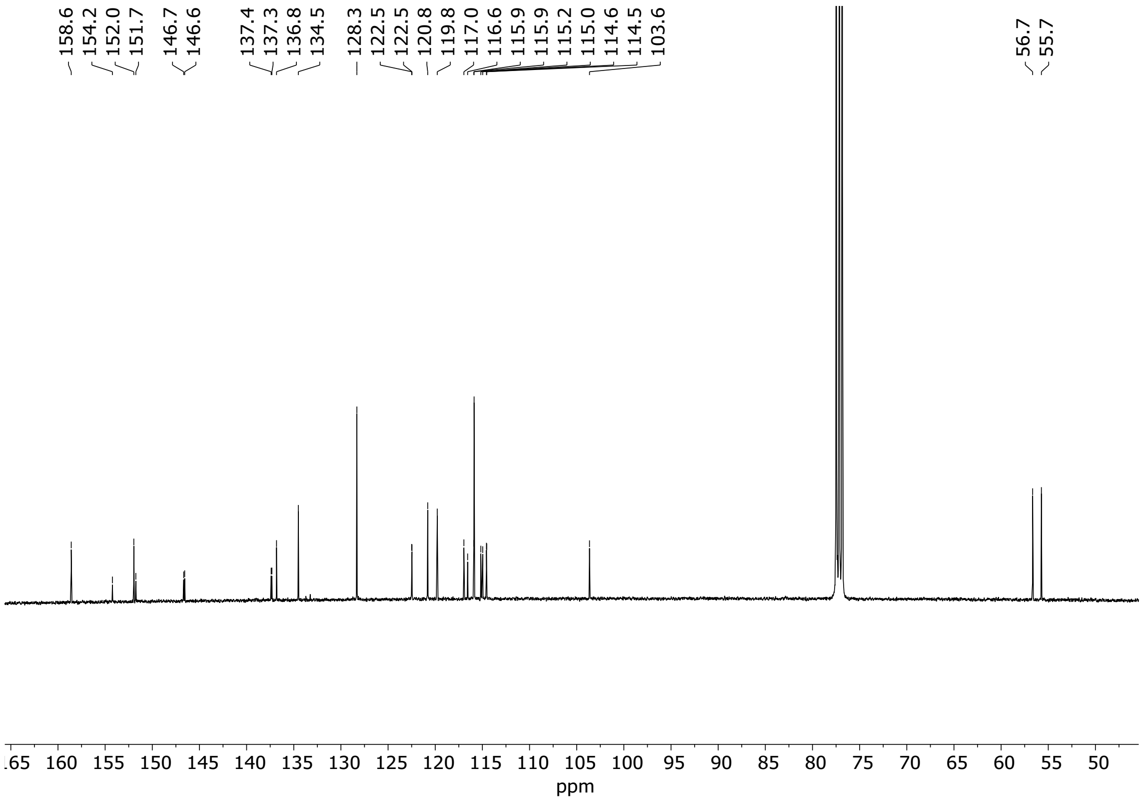

Figure S4. ^{13}C-NMR of **2** in $CDCl_3$.

Characterization of ZnPc-1

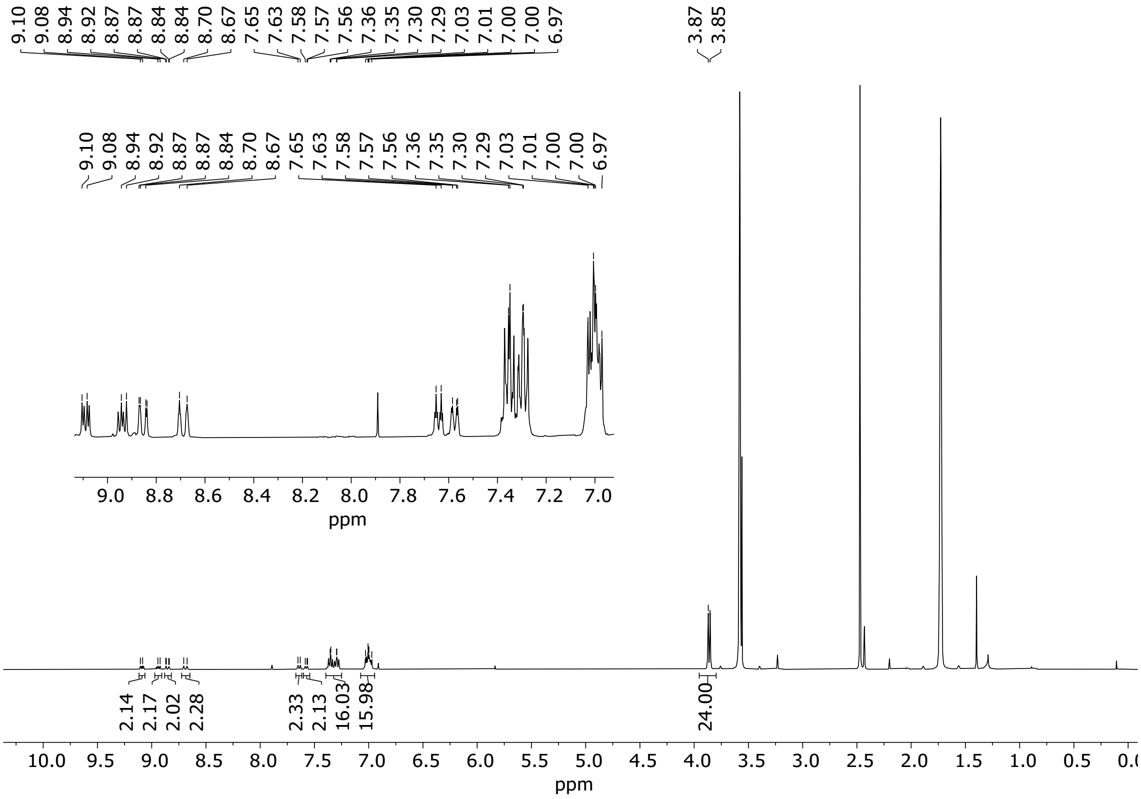

Figure S5. [1]H-NMR of **ZnPc-1** in THF-d_8.

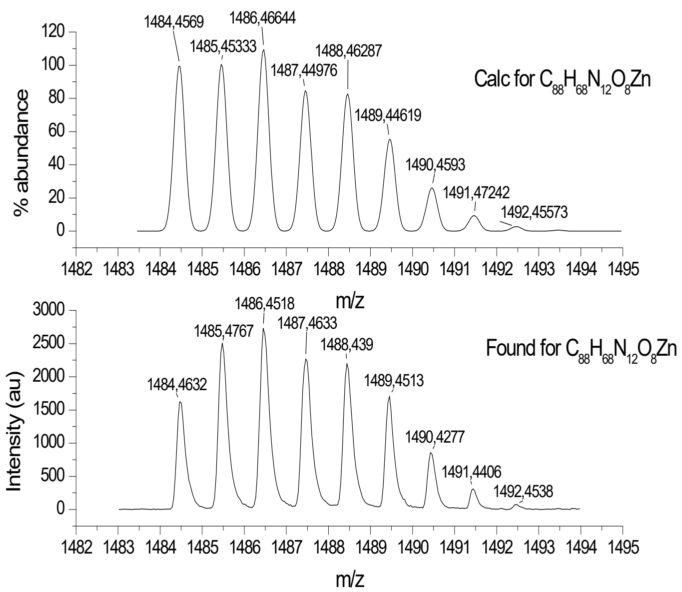

Figure S6. HR-MALDI-TOF spectrum of **ZnPc-1**.

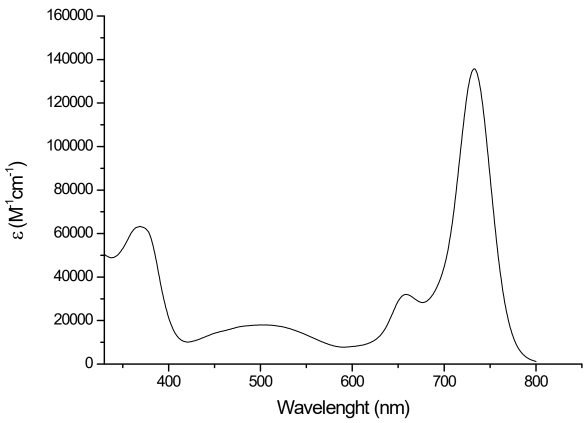

Figure S7. Uv-vis absorption spectra of **ZnPc-1** in DMF.

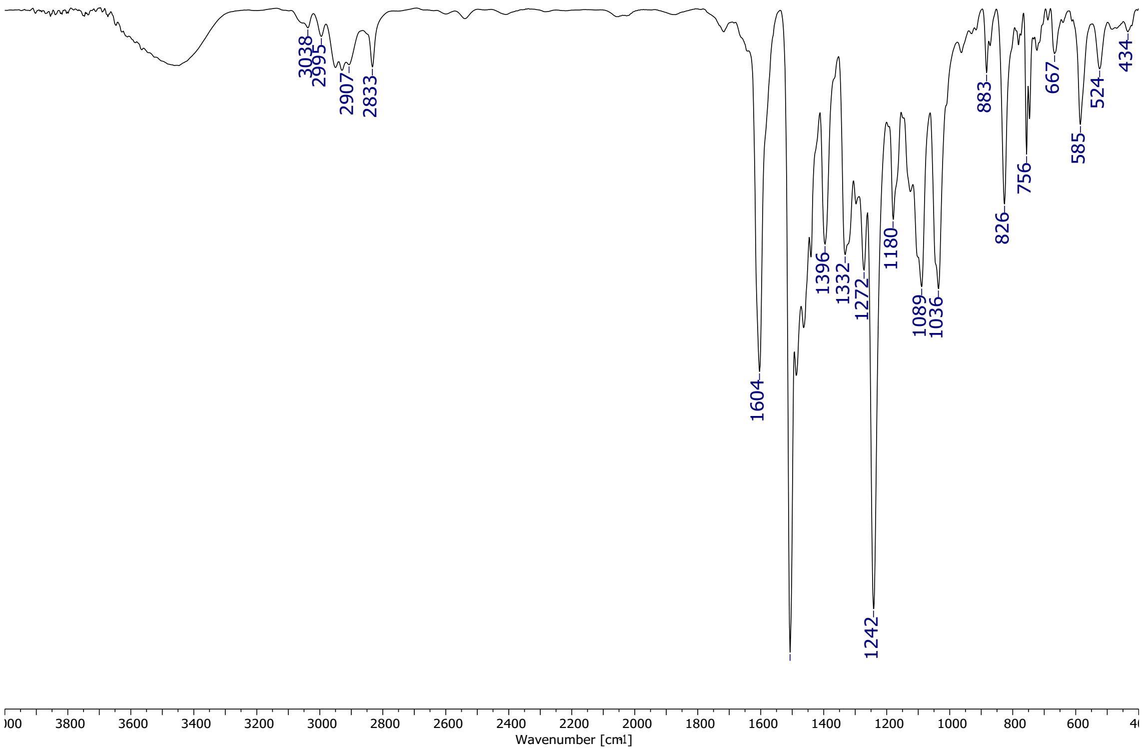

Figure S8. FT-IR of **ZnPc-1**.

Characterization of ZnPc-2

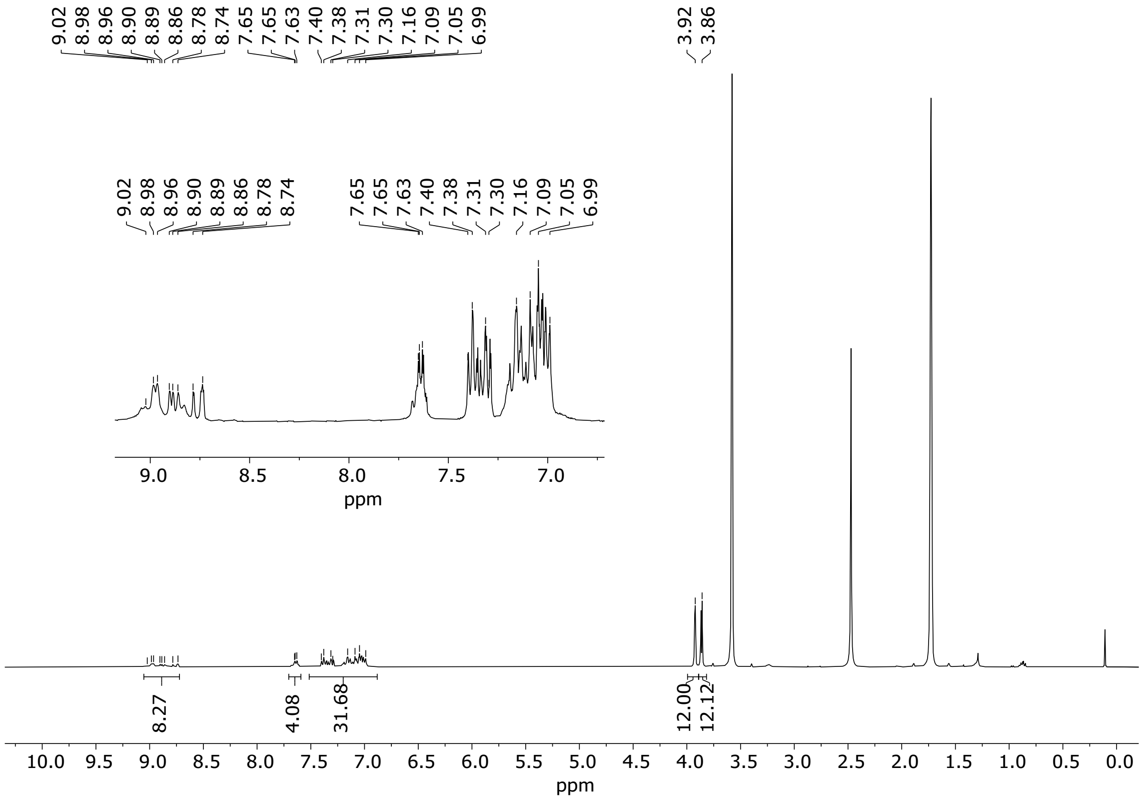

Figure S9. ^{1}H-NMR of **ZnPc-2** in THF-d_8.

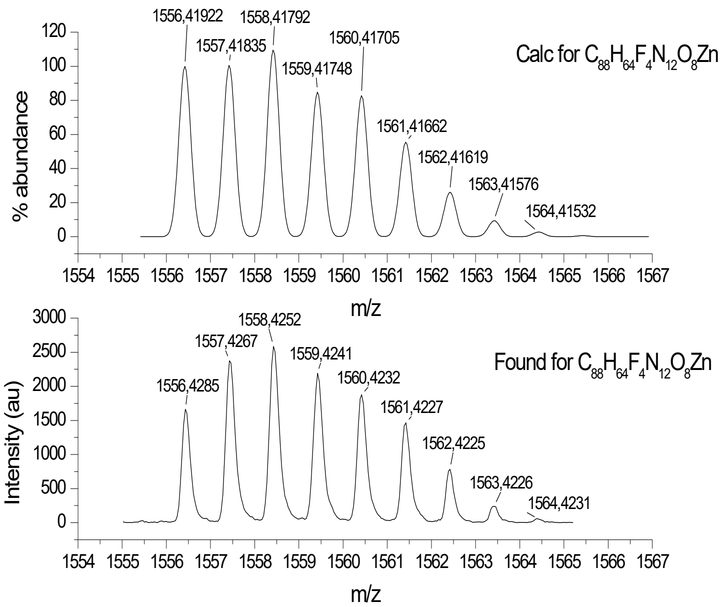

Figure S10. HR-MALDI-TOF spectrum of **ZnPc-2**.

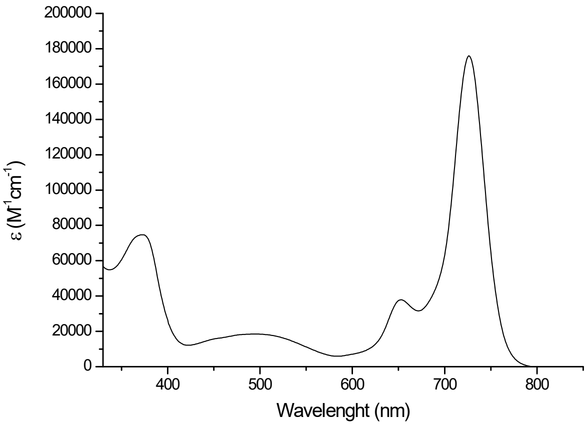

Figure S11. UV-vis absorption spectra of **ZnPc-2** in DMF.

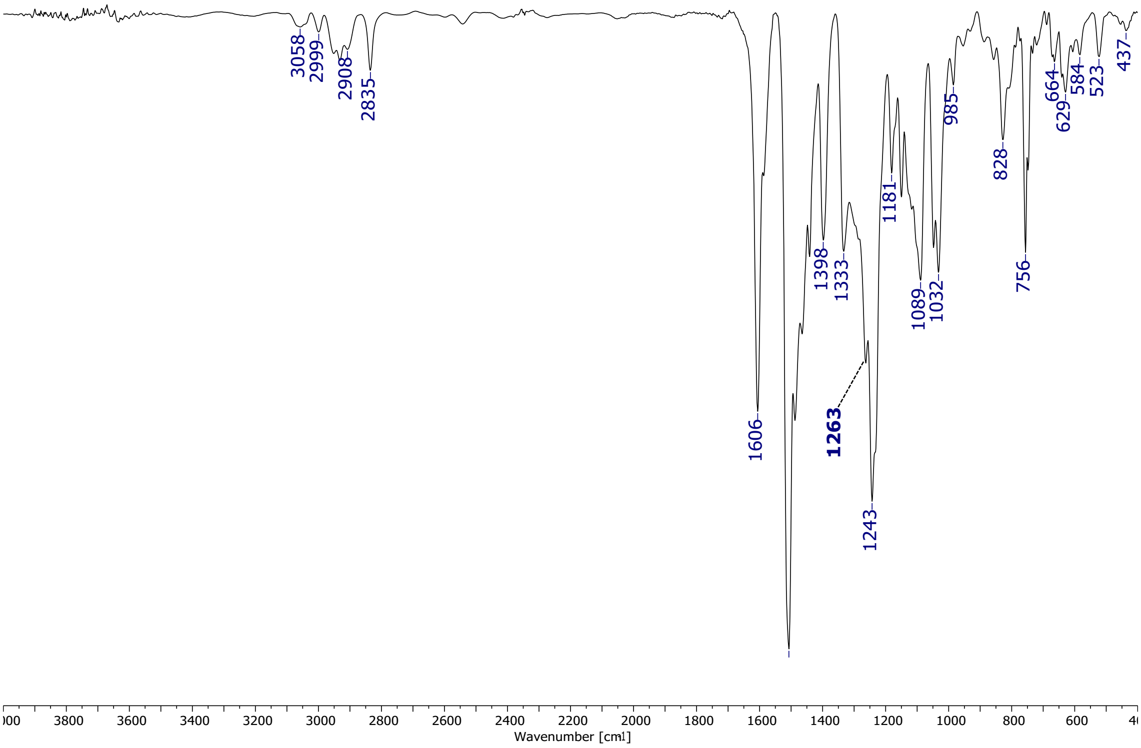

Figure S12. FT-IR of **ZnPc-2**.

Characterization of CuPc-3

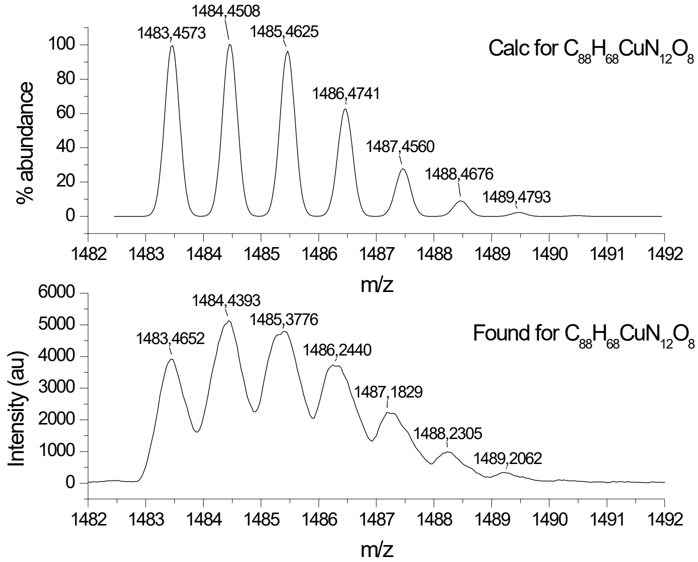

Figure S13. HR-MALDI-TOF spectrum of **CuPc-3**.

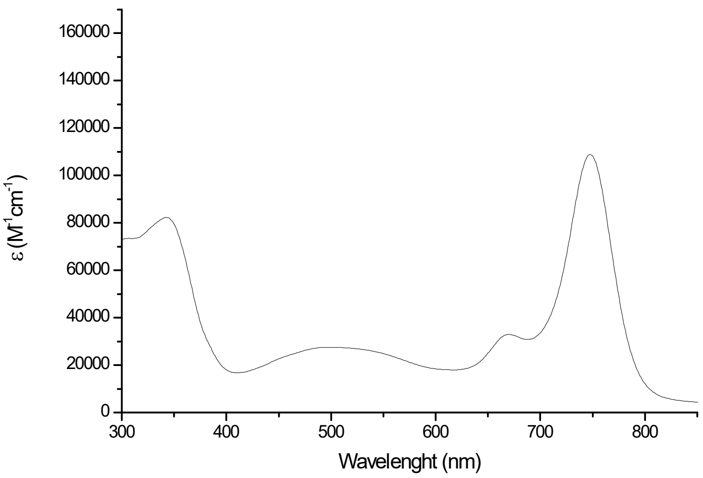

Figure S14. Uv-vis absorption spectra of **CuPc-3** in DMF.

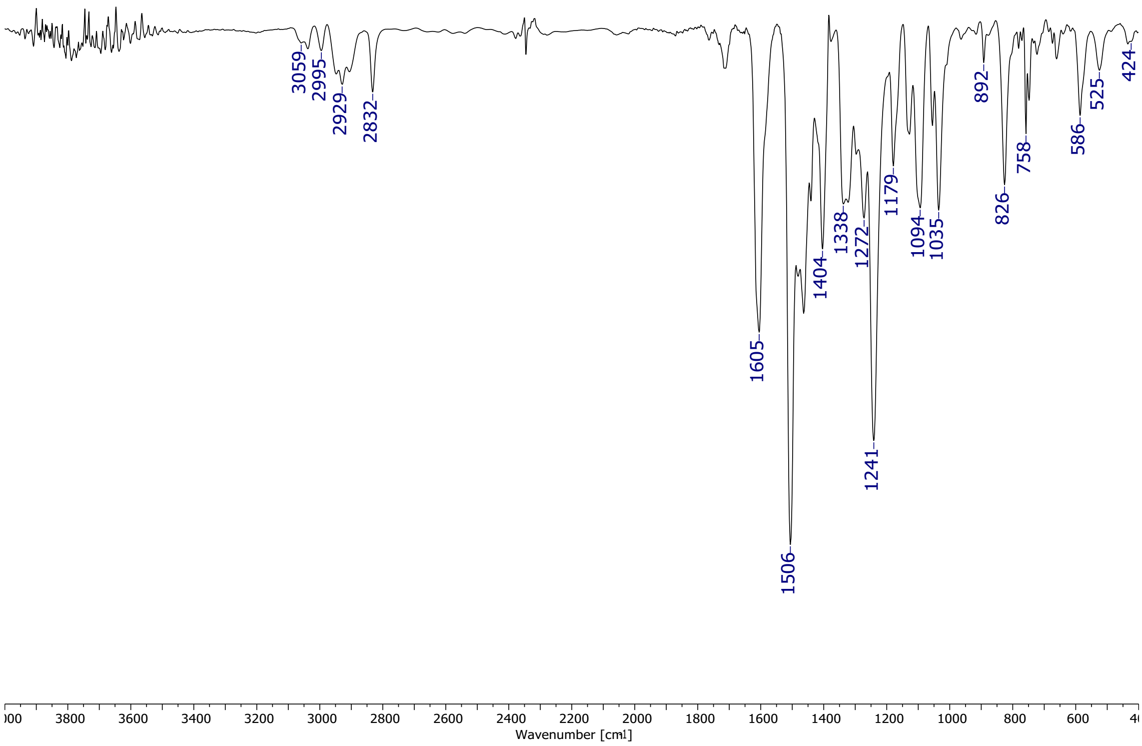

Figure S15. FT-IR of **CuPc-3.**

Characterization of CuPc-4

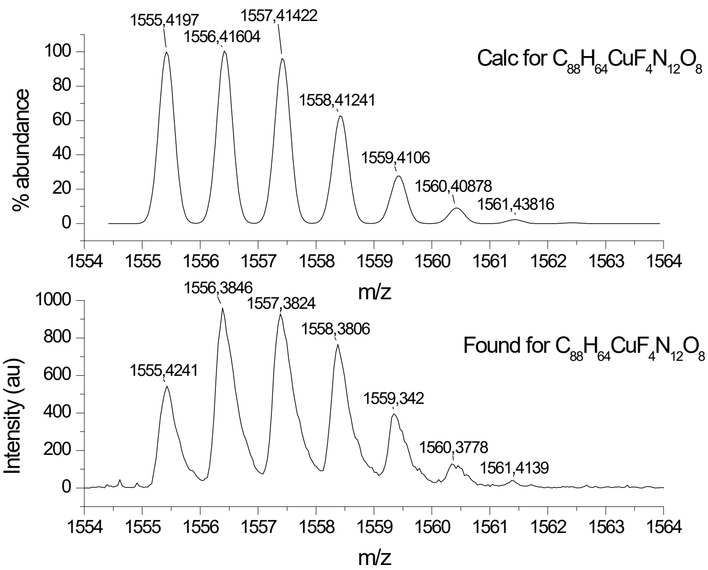

Figure S16. HR-MALDI-TOF spectrum of **CuPc-4.**

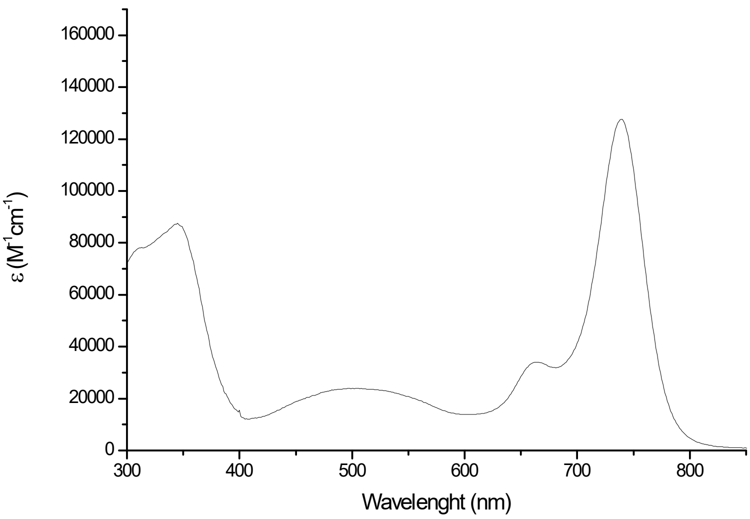

Figure S17. UV-vis absorption spectra of **CuPc-4** in DMF.

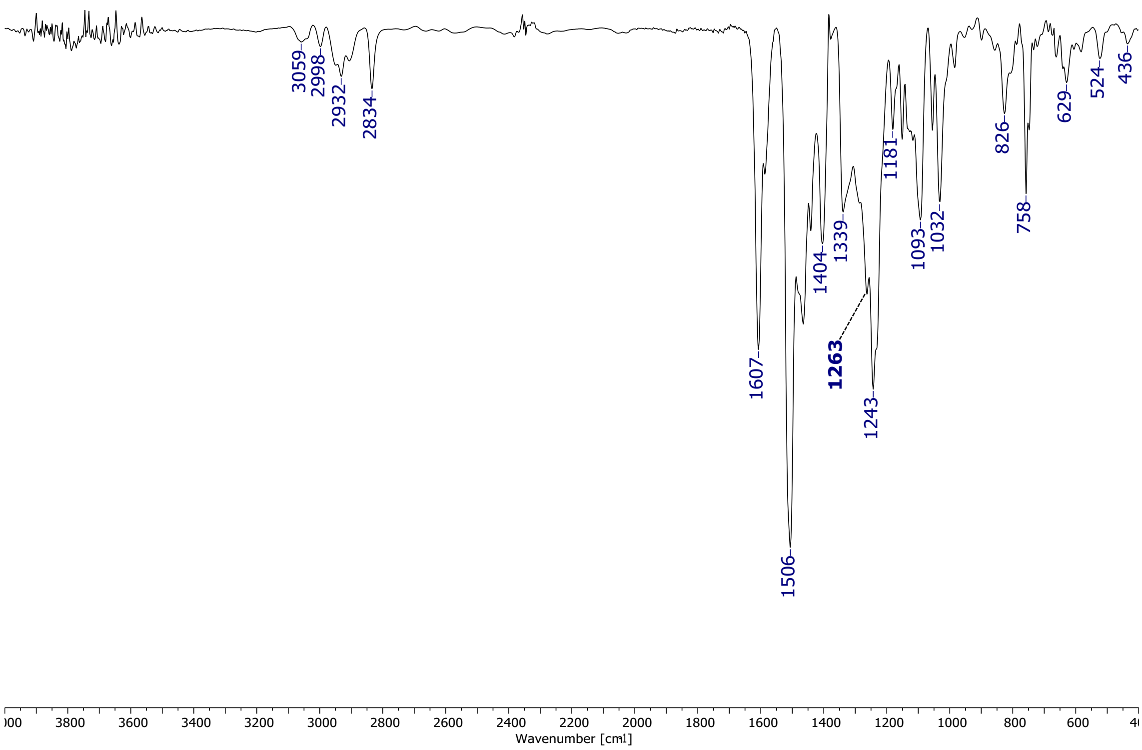

Figure S18. FT-IR of **CuPc-4**.

Characterization of ZnPc-5

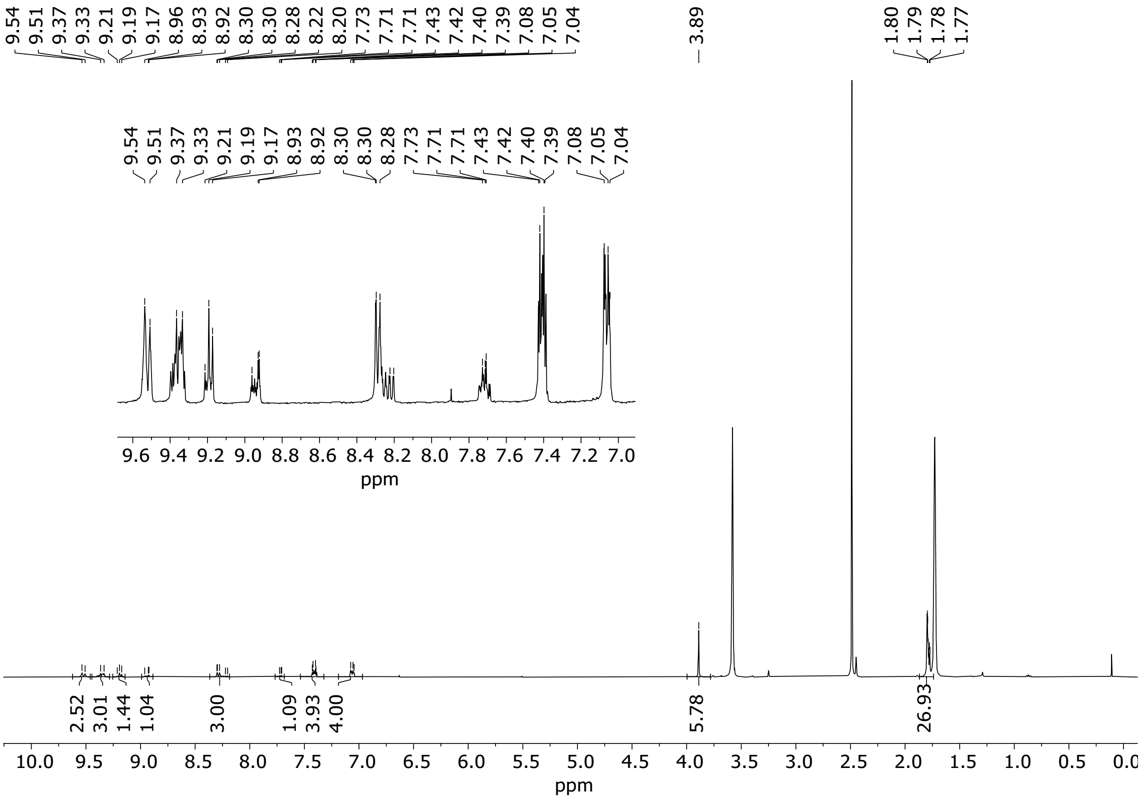

Figure S19. [1]H-NMR of **ZnPc-5** in THF-d_8.

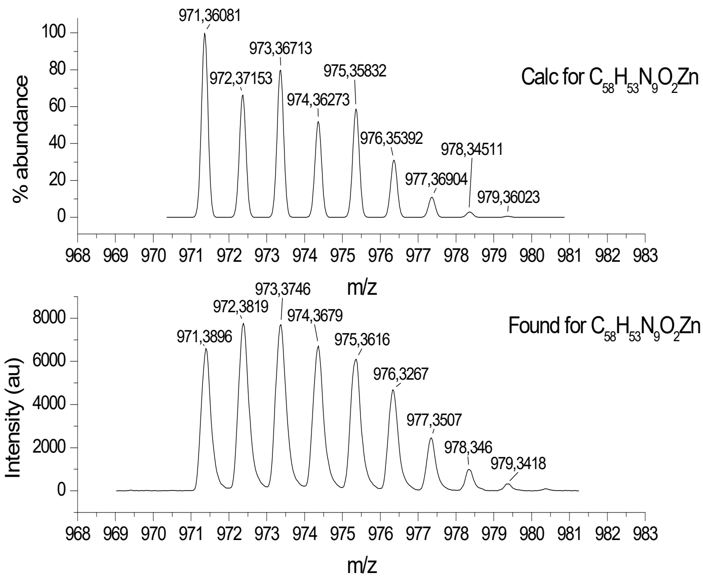

Figure S20. HR-MALDI-TOF spectrum of **ZnPc-5**.

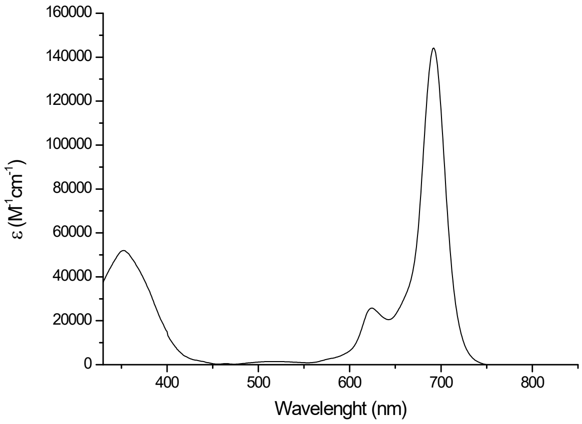

Figure S21. UV-vis absorption spectra of **ZnPc-5** in DMF.

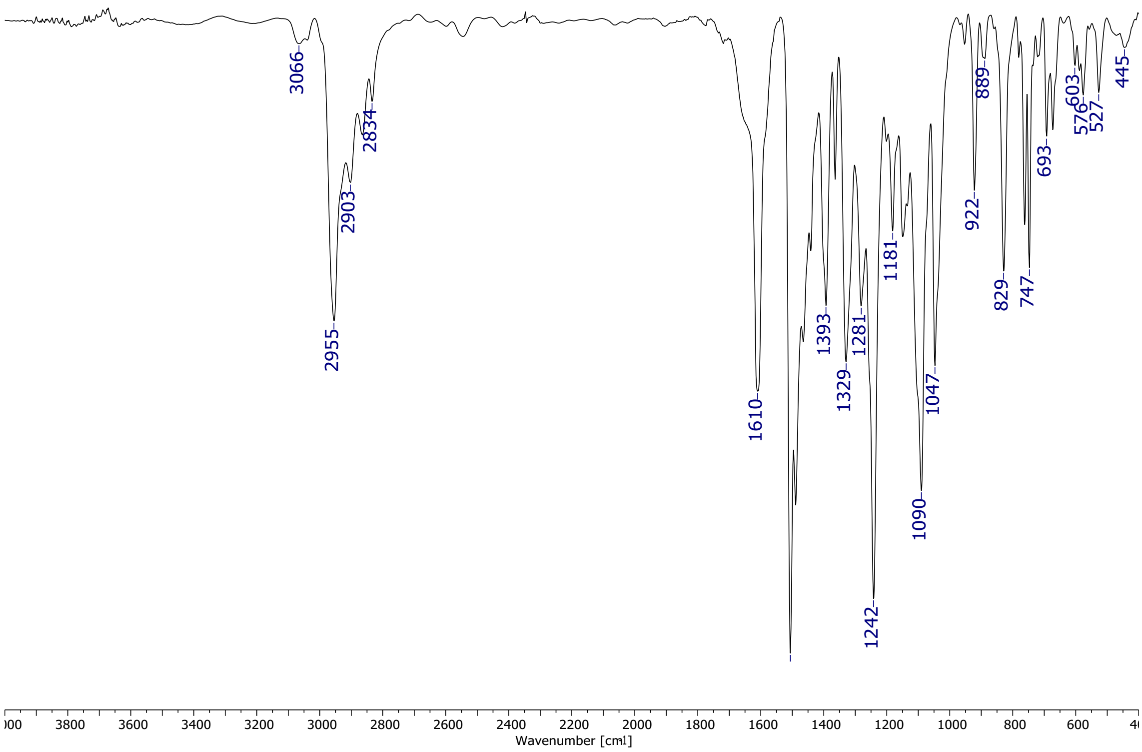

Figure S22. FT-IR of **ZnPc-5**.

Characterization of ZnPc-6

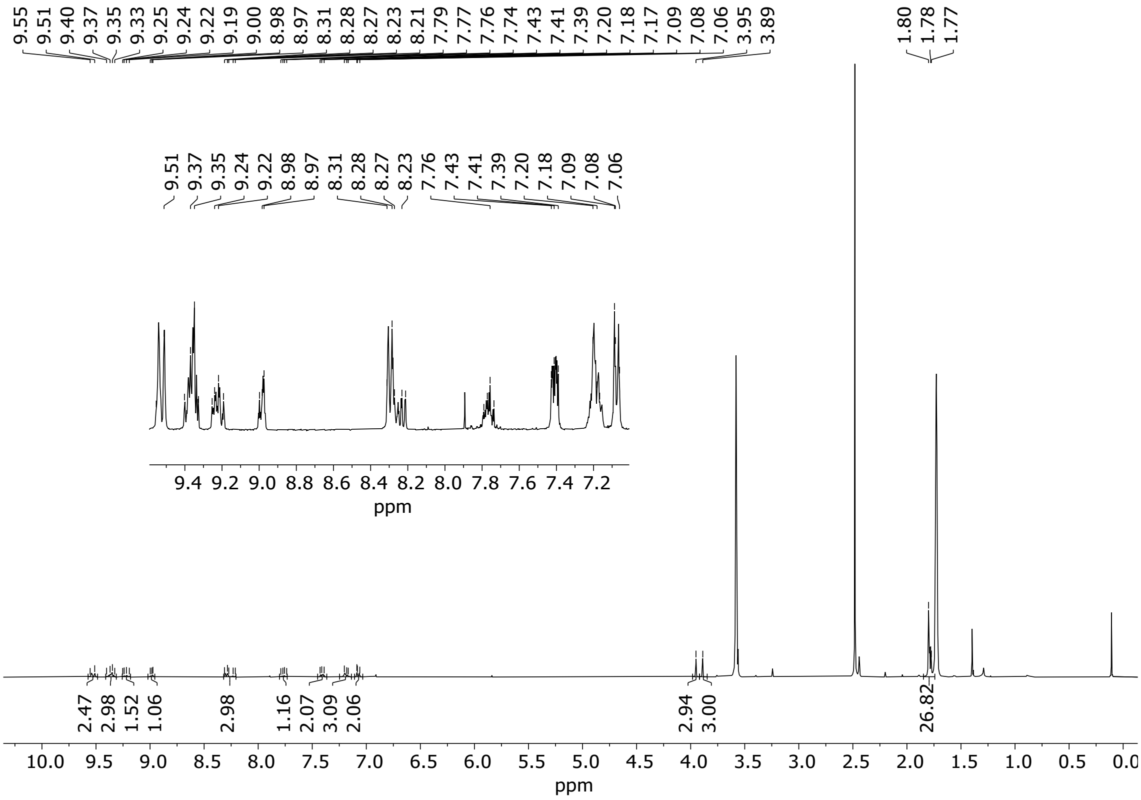

Figure S23. ^{1}H-NMR of **ZnPc-6** in THF-d_8.

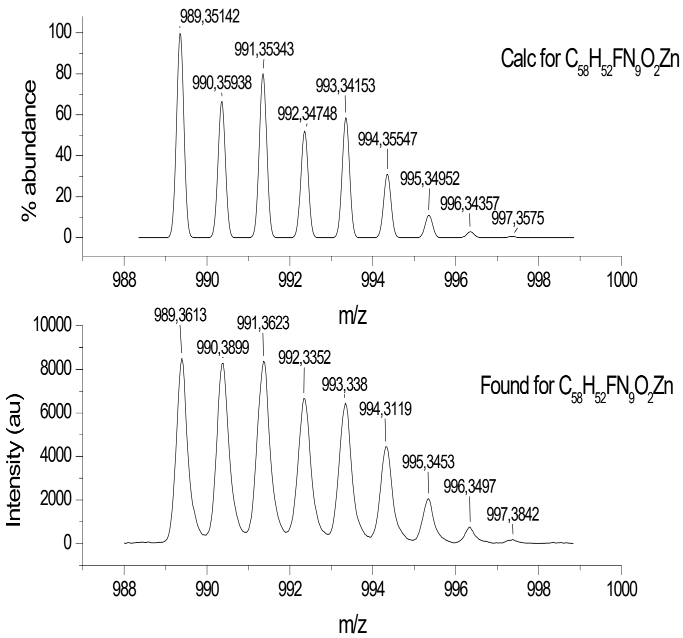

Figure S24. HR-MALDI-TOF spectrum of **ZnPc-6**.

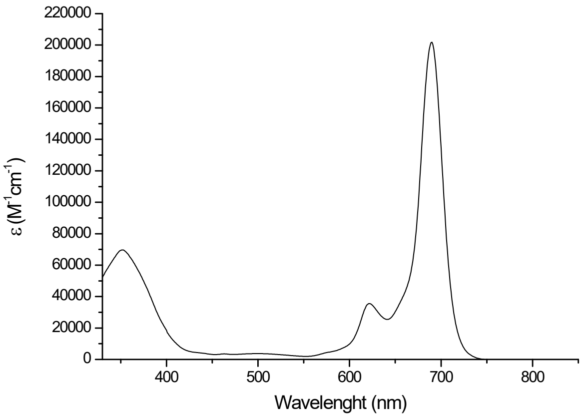

Figure S25. UV-vis absorption spectra of **ZnPc-6** in DMF.

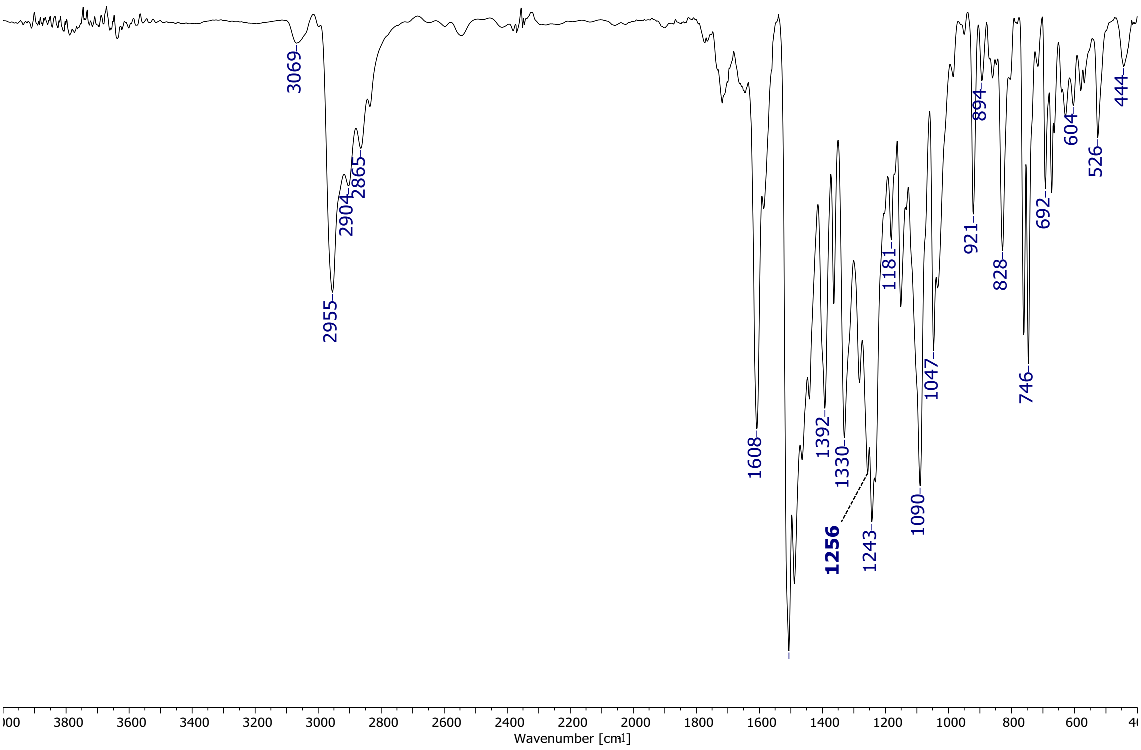

Figure S26. FT-IR of **ZnPc-6**.

Characterization of CuPc-7

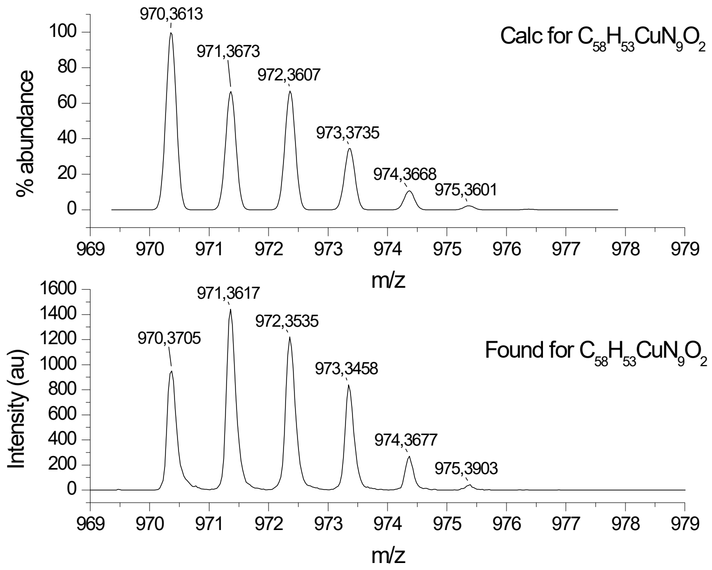

Figure S27. HR-MALDI-TOF spectrum of **CuPc-7**.

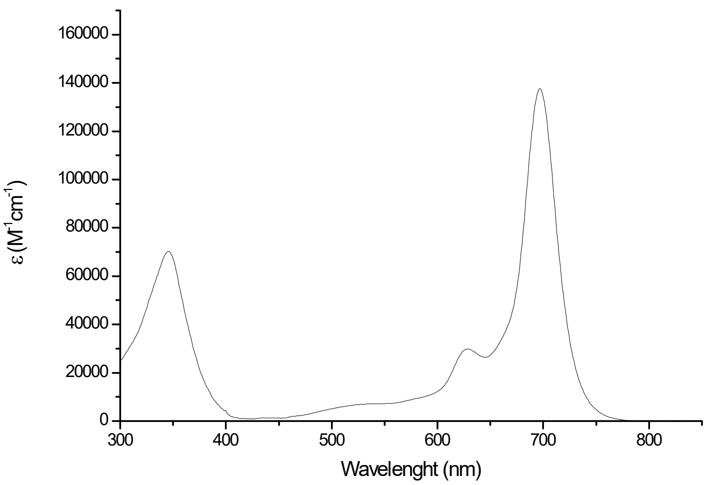

Figure S28. UV-vis absorption spectra of **CuPc-7** in DMF.

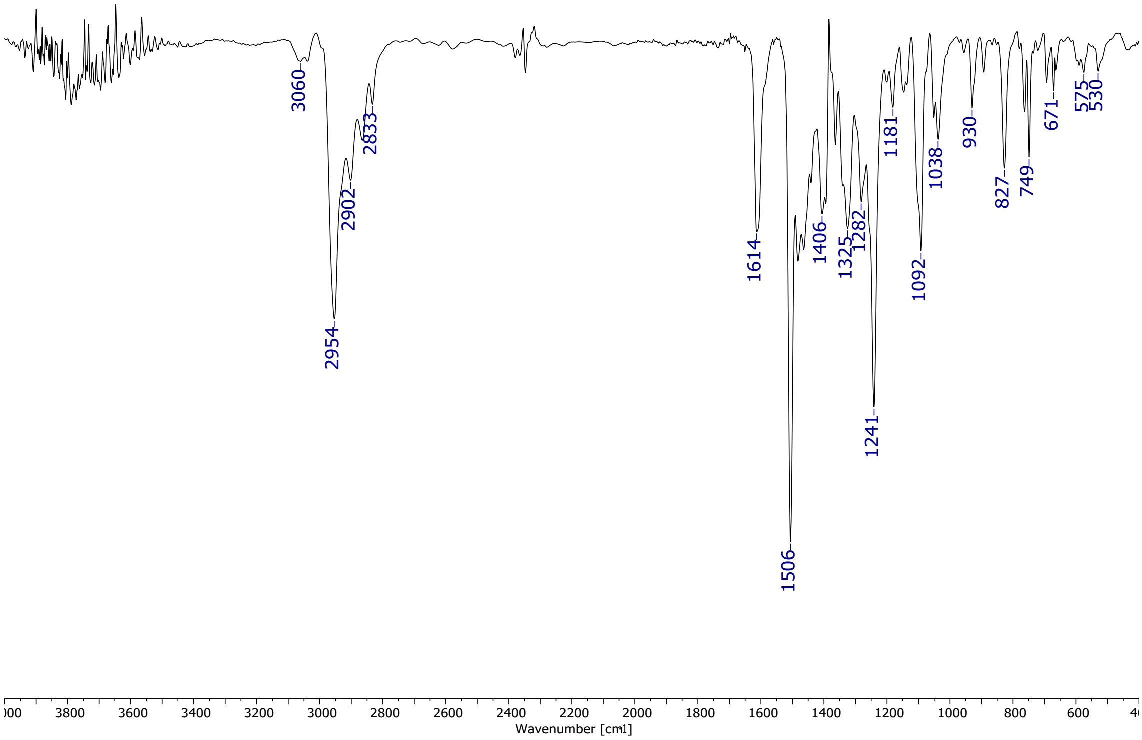

Figure S29. FT-IR of **CuPc-7**.

Characterization of CuPc-8

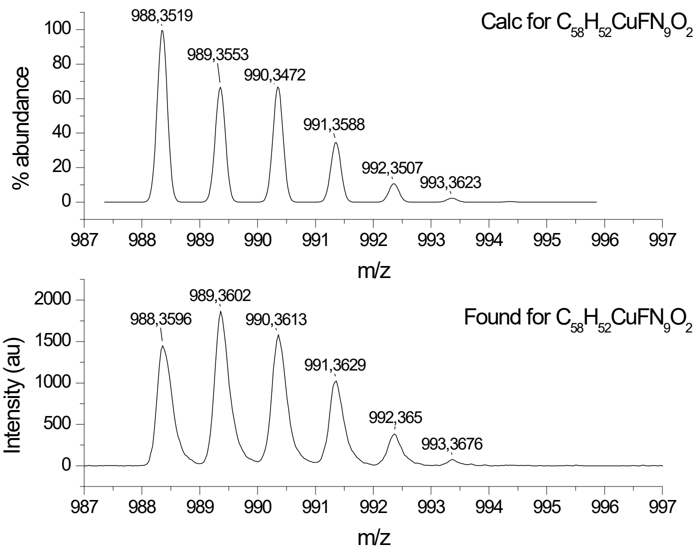

Figure S30. HR-MALDI-TOF spectrum of **CuPc-8**.

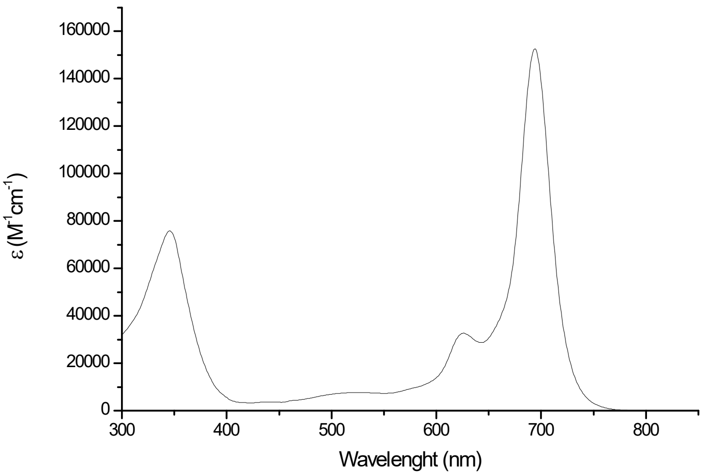

Figure S31. UV-vis absorption spectra of **CuPc-8** in DMF.

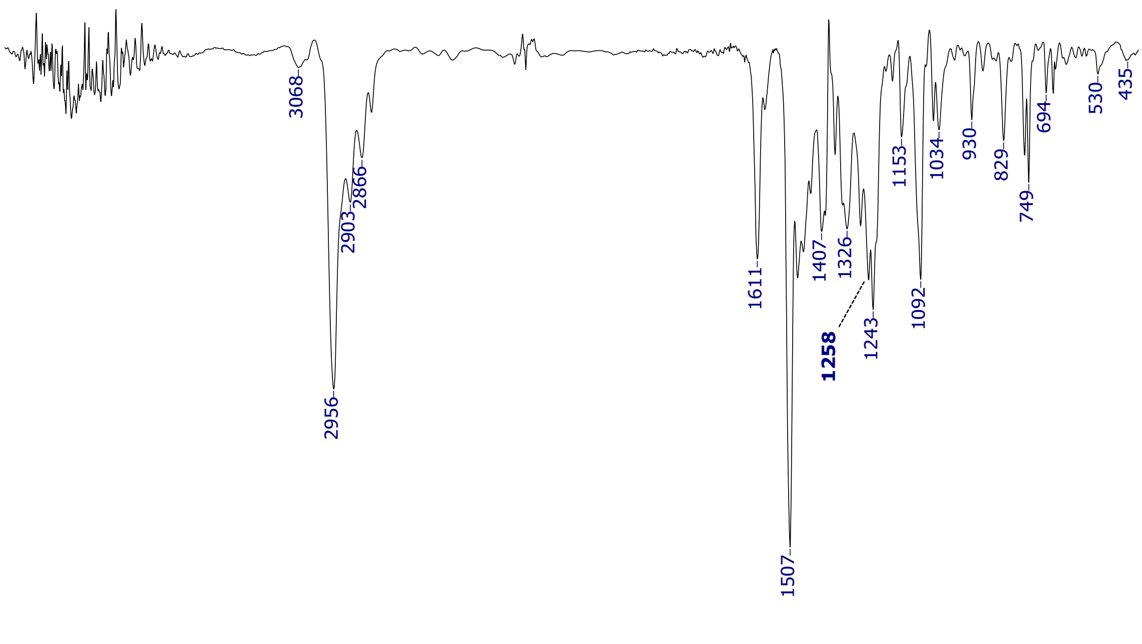

Figure S32. FT-IR of **CuPc-8**.

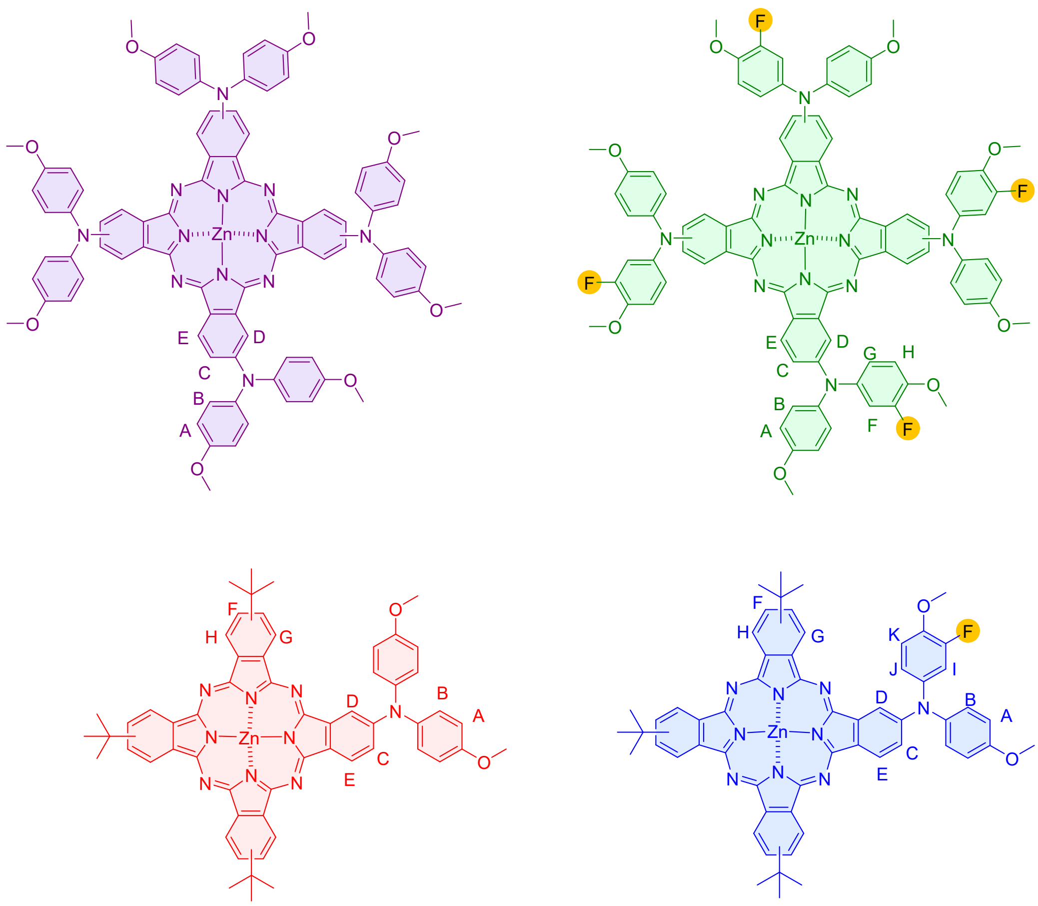

Figure S33. ^{1}H-NMR assignation of protons for **ZnPc -1** (purple), **-2** (green), **-5** (red), and **-6** (blue).

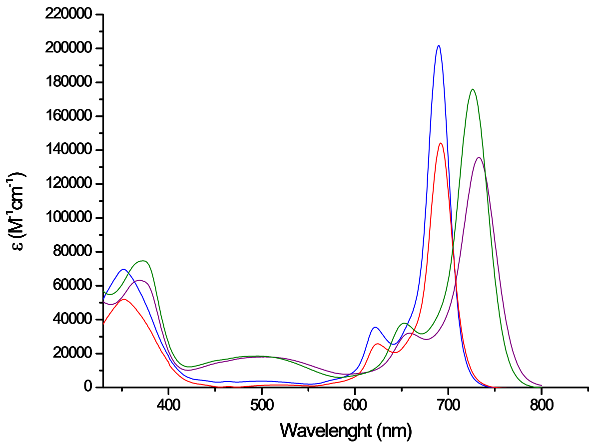

Figure S34. UV-vis absorption spectra of **ZnPc -1** (purple), **-2** (green), **-5** (red), and **-6** (blue).

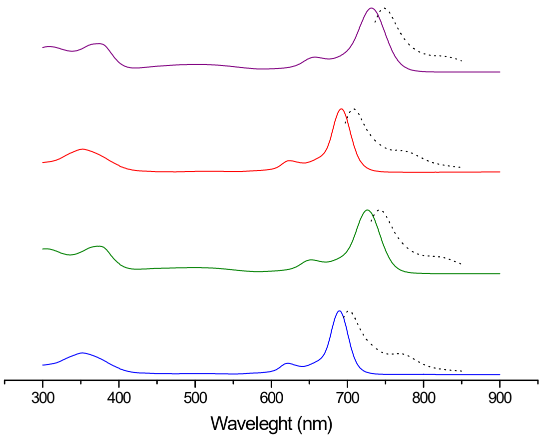

Figure S35. Normalized UV-vis absorption (solid line) and fluorescence (dotted line) spectra of **ZnPc -1** (purple), **-2** (green), **-5** (red), and **-6** (blue).

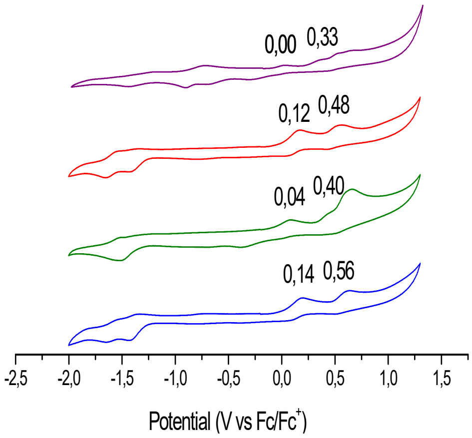

Figure S36. Cyclic voltammogram of **ZnPc -1** (purple), **-2** (green), **-5** (red), and **-6** (blue).

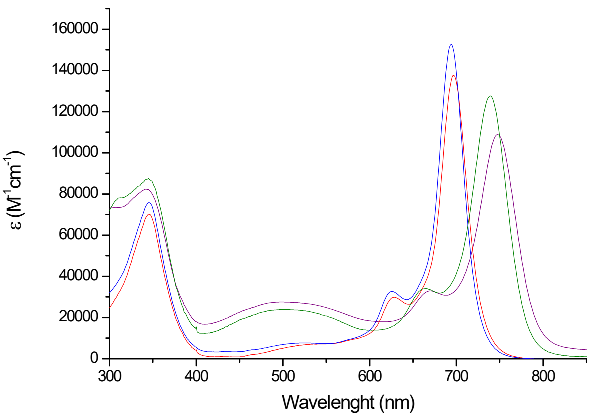

Figure S37. UV-vis absorption spectra of CuPc -**3** (purple), **-4** (green), **-7** (red), and **-8** (blue).

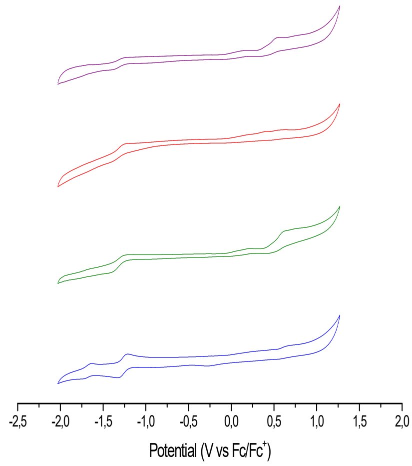

Figure S38. Cyclic voltammogram of CuPc -**3** (purple), -**4** (green), -**7** (red), and -**8** (blue).

Electrochemistry

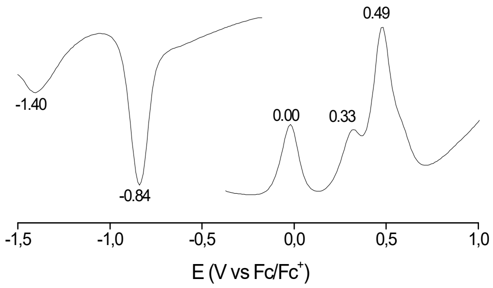

Figure S39. Differential pulse voltammetry of ZnPc-1 in deaerated DMF solution containing $TBAPF_6$ (0.1 M) obtained at 298 K.

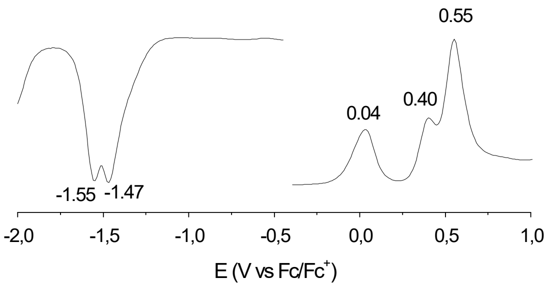

Figure S40. Differential pulse voltammetry of ZnPc-2 in deaerated DMF solution containing TBAPF6 (0.1 M) obtained at 298 K.

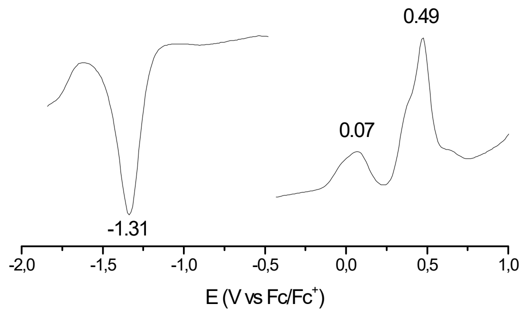

Figure S41. Differential pulse voltammetry of CuPc-3 in deaerated DMF solution containing TBAPF6 (0.1 M) obtained at 298 K.

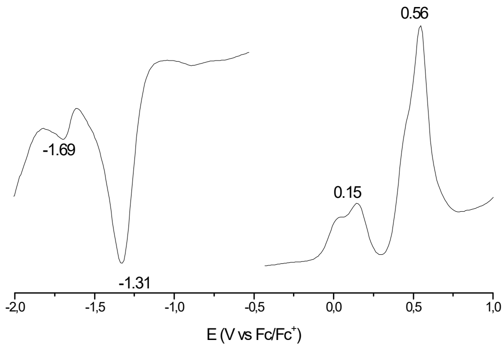

Figure S42. Differential pulse voltammetry of CuPc-4 in deaerated DMF solution containing TBAPF6 (0.1 M) obtained at 298 K.

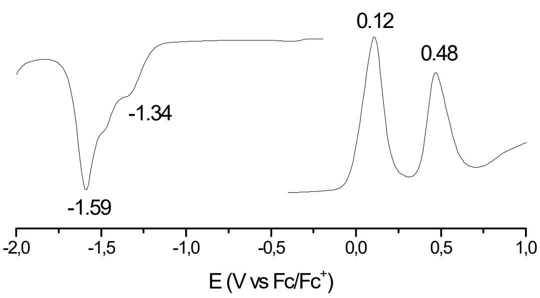

Figure S43. Differential pulse voltammetry of ZnPc-5 in deaerated DMF solution containing TBAPF6 (0.1 M) obtained at 298 K.

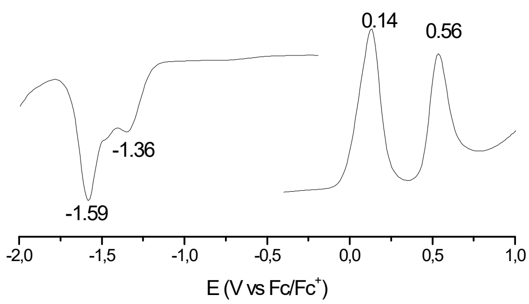

Figure S44. Differential pulse voltammetry of ZnPc-6 in deaerated DMF solution containing TBAPF6 (0.1 M) obtained at 298 K.

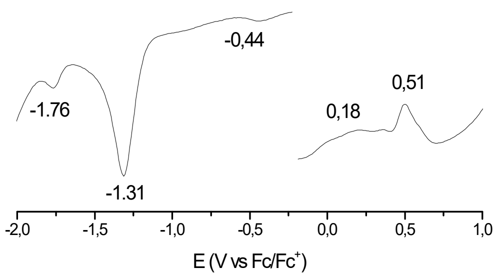

Figure S45. Differential pulse voltammetry of CuPc-7 in deaerated DMF solution containing TBAPF6 (0.1 M) obtained at 298 K.

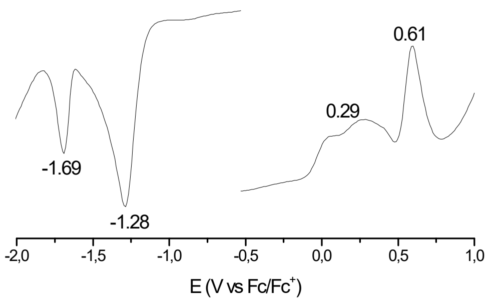

Figure S46. Differential pulse voltammetry of CuPc-8 in deaerated DMF solution containing TBAPF6 (0.1 M) obtained at 298 K.

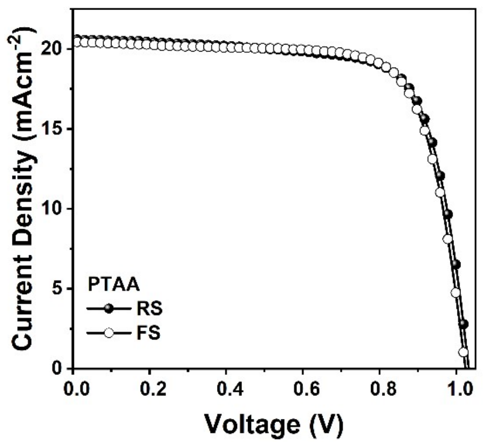

Figure S47. Reverse and forward scan *J-V* curves for PSC based on pristine PTAA as HTM.

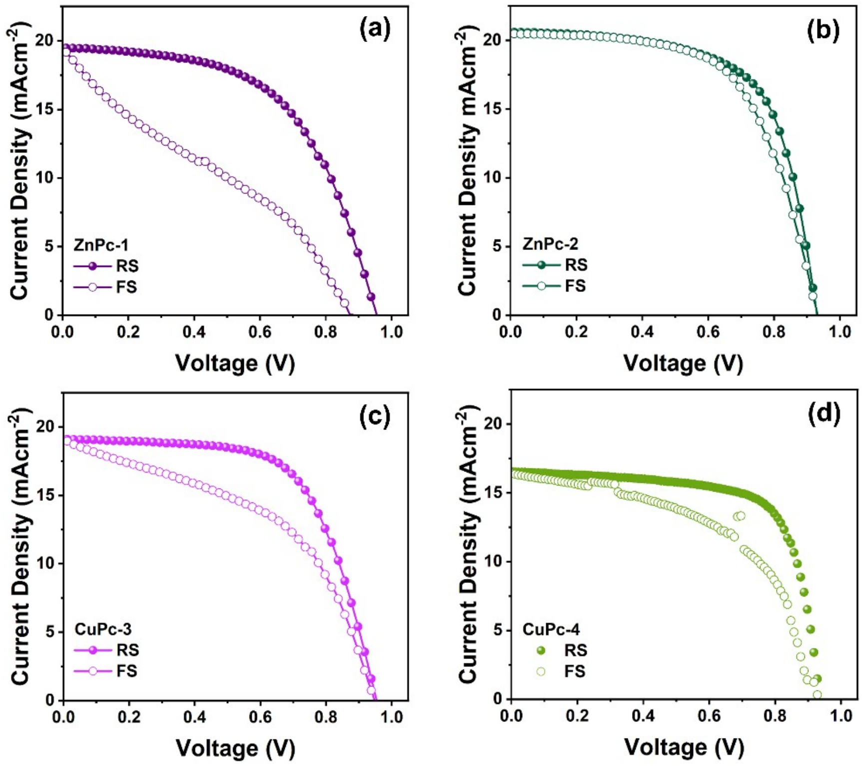

Figure S48. Reverse and forward scan *J-V* curves for PSCs based on symmetrical MPcs, (a) ZnPc-1, (b) ZnPc-2, (3) CuPc-3, and (4) CuPc-4.

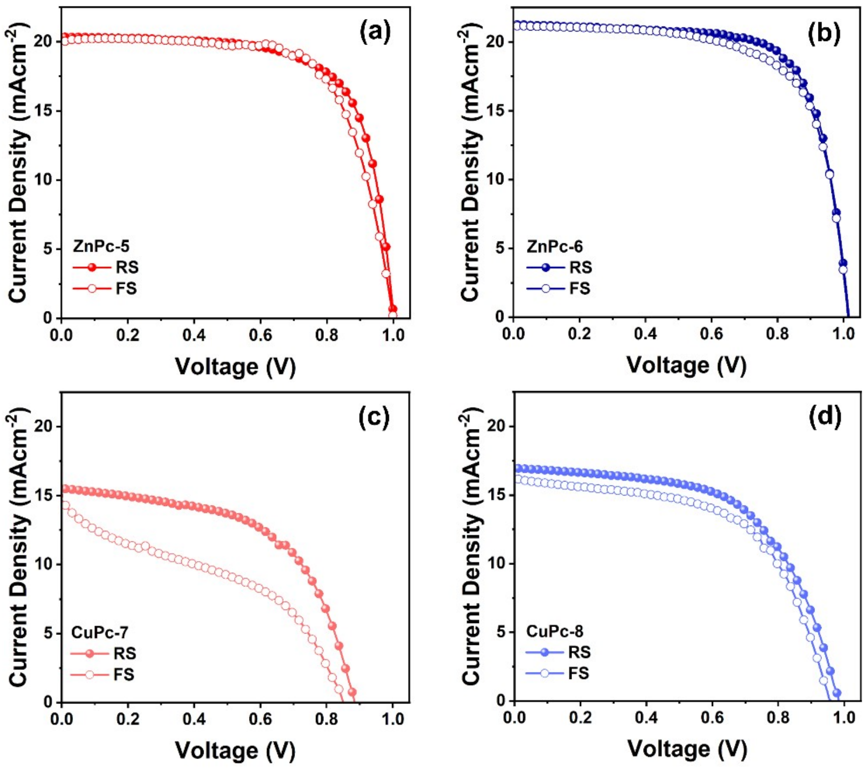

Figure S49. Reverse and forward scan *J-V* curves for PSCs based on symmetrical MPcs, (a) ZnPc-5, (b) ZnPc-6, (3) CuPc-7, and (4) CuPc-8.

Table S1. Statistical data of *J-V* parameters of champion devices based on *n-i-p* configuration.

HTM	V_{oc} (mV)	J_{sc} (mAcm^{-2})	FF (%)	PCE (%)	*HI
ZnPc-1	890.54±48.83	17.89±1.08	54.21±8.31	8.59±1.22	0.5058
ZnPc-2	936.01±7.43	20.08±0.29	63.39±1.81	11.92±0.47	0.0750
CuPc-3	962.83±17.17	17.36±1.18	63.38±2.75	10.58±0.68	0.2549
CuPc-4	930.26±15.24	16.66±0.60	60.99±7.36	9.45±1.15	0.1486
ZnPc-5	995.24±5.77	20.01±0.26	69.55±0.89	13.85±0.34	0.0550
ZnPc-6	1011.98±4.04	20.94±0.18	70.03±1.16	14.84±0.37	0.0415
CuPc-7	833.46±58.74	10.98±2.84	50.39±7.59	4.56±1.37	0.3542
CuPc-8	881.8±48.27	15.10±1.58	52.36±8.47	6.96±1.38	0.0773

*HI = [$PCE_{RS} - PCE_{FS}$]/PCE_{RS}, where PCE_{RS} and PCE_{FS} represent the PCE from reverse and forward scans, respectively. Statistical distribution was calculated from 8 devices of each ZnPc-1, CuPc-4, CuPc-7, CuPc-8, and 10 devices of each ZnPc-2, CuPc-3, ZnPc-5, ZnPc-6.

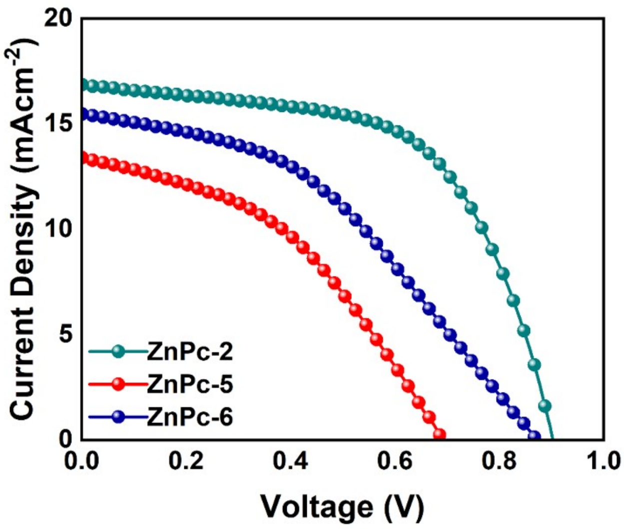

Figure S50. J-V curves in the reverse scan for *p-i-n* devices based on ZnPc-2, ZnPc-5, and ZnPc-6.

Table S2. Performance summary of devices based on *p-i-n* configuration with ZnPc-2, ZnPc-5, and ZnPc-6.

HTM	V_{oc} (mV)	J_{sc} (mAcm^{-2})	FF ((%)	PCE (%)	R_s (Ω)	R_{sh} (kΩ)
ZnPc-2	901.87	16.85	59.59	9.06	98.86	4.379
ZnPc-5	693.94	13.41	41.74	3.88	300.88	1.880
ZnPc-6	865.26	15.48	41.28	5.53	311.79	2.604

Table S3. Performance summary of devices based on *p-i-n* configuration with ZnPc-2, ZnPc-5, and ZnPc-6.

HTM	Conductivity (S/cm)	Mobility (cm^2/Vs)
ZnPc-1	4.660×10^{-7}	8.994×10^{-6}
ZnPc-2	1.210×10^{-6}	3.199×10^{-5}
CuPc-3	8.121×10^{-7}	8.150×10^{-6}
CuPc-4	8.024×10^{-7}	1.051×10^{-5}
ZnPc-5	1.045×10^{-6}	1.949×10^{-5}
ZnPc-6	1.268×10^{-6}	2.039×10^{-5}

CuPc-7	8.142×10^{-7}	6.335×10^{-5}
CuPc-8	7.688×10^{-7}	3.434×10^{-5}

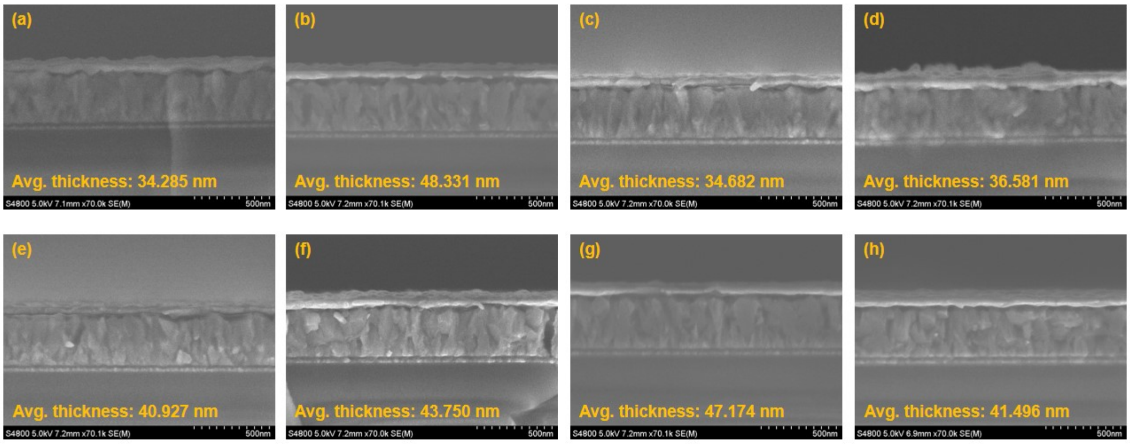

Figure S51. Cross-sectional SEM images of FTO/MPc/Ag devices and average thickness of each MPc.

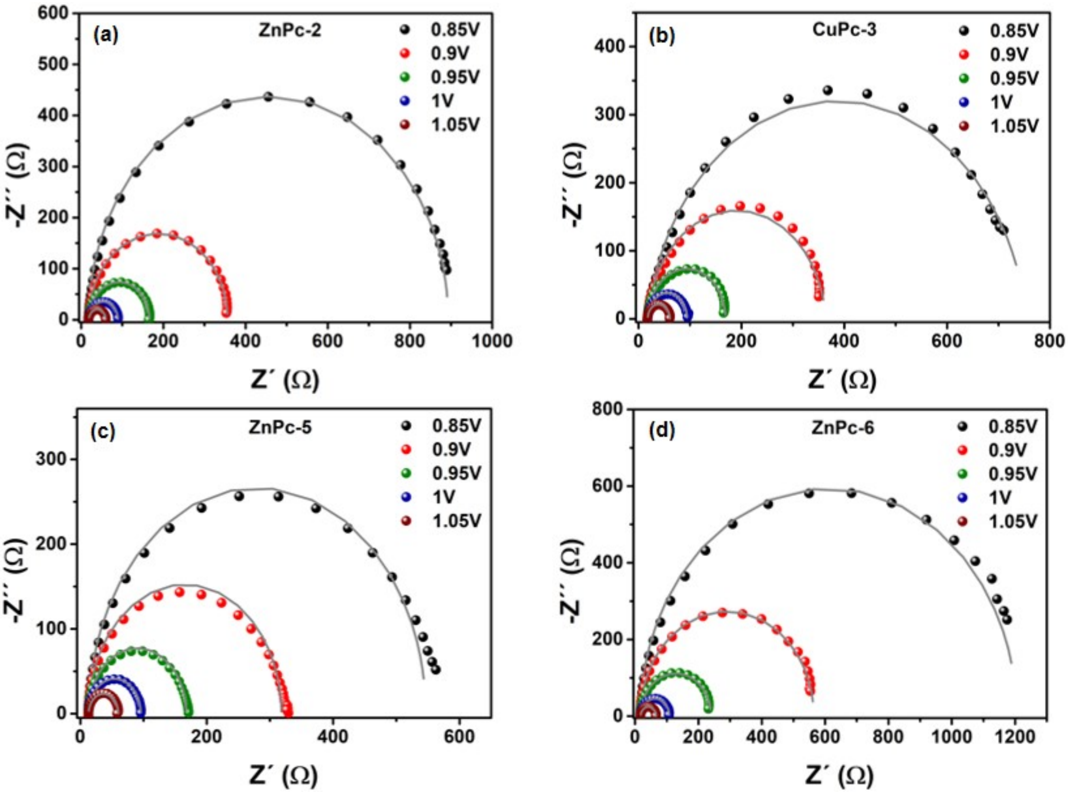

Figure S52. Electrochemical impedance spectra (EIS) of PSCs based on ZnPc-2, CuPc-3, ZnPc-5, and ZnPc-6 measured at different bias voltages from 0.85–1.05 V under dark conditions (raw and fitted data).

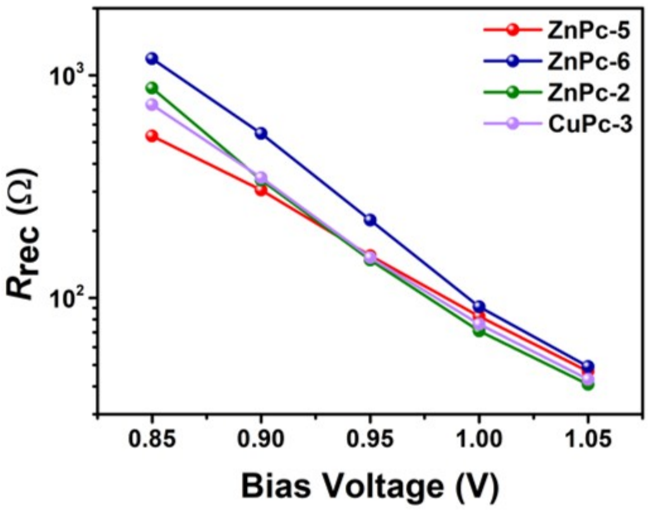

Figure S53. The bias voltage-dependent interfacial charge recombination resistance extracted from Nyquist plots under dark conditions.